

Sayiter YILDIZ<sup>1</sup>

## ARTIFICIAL NEURAL NETWORK APPROACH FOR MODELING OF Ni(II) ADSORPTION FROM AQUEOUS SOLUTION BY PEANUT SHELL

### WYKORZYSTANIE SZTUCZNYCH SIECI NEURONOWYCH DO MODELOWANIA ADSORPCJI Ni(II) Z ROZTWORÓW WODNYCH PRZEZ SKORUPKI ORZECHÓW ARACHIDOWYCH

**Abstract:** In this study, ANN (artificial neural network) model was applied to estimate the Ni(II) removal efficiency of peanut shell based on batch adsorption tests. The effects of initial pH, metal concentrations, temperature, contact time and sorbent dosage were determined. Also, *COD* (chemical oxygen demand) was measured to evaluate the possible adverse effects of the sorbent during the tests performed with varying temperature, pH and sorbent dosage. *COD* was found as 96.21 mg/dm<sup>3</sup> at pH 2 and 54.72 mg/dm<sup>3</sup> at pH 7. Also, a significant increase in *COD* value was observed with increasing dosage of the used sorbent. *COD* was found as 12.48 mg/dm<sup>3</sup> after use of 0.05 g sorbent and as 282.78 mg/dm<sup>3</sup> after use of 1 g sorbent. During isotherm studies, the highest regression coefficient ( $R^2$ ) value was obtained with Freundlich isotherm ( $R^2 = 0.97$ ) for initial concentration and with Temkin isotherm for sorbent dosage. High pseudo-second order kinetic model regression constants were observed ( $R^2 = 0.95-0.99$ ) during kinetic studies with varying pH values. In addition, Ni(II) ion adsorption on peanut shell was further defined with pseudo-second order kinetic model, since  $q_e$  values in the second order kinetic equation were very close to the experimental values. The relation between the estimated results of the built ANN model and the experimental results were used to evaluate the success of ANN modeling. Consequently, experimental results of the study were found to be in good agreement with the estimated results of the model.

**Keywords:** artificial neural network, isotherm study, equilibrium, Ni(II) ions

## Introduction

Ever-increasing world population and consequently increasing demands have led to increased industrial activities throughout the world. Heavy metals are the most common contaminants which are found in high concentrations in the content of industrial waste waters. Due to their detrimental physiological effects on living creatures [1], which arise from their indissoluble molecular structures, presence of these metals in aquatic environment and industrial waste sites poses an important environmental problem [2]. Removal of heavy metals is a worldwide environmental concern which has become

---

<sup>1</sup> Department of Environmental Engineering, Engineering Faculty, Cumhuriyet University, Kayseri street, 58140, Sivas, Turkey, phone +90 03462191010, email: sayiteryildiz@gmail.com

prevalent particularly in developing and industrialized countries [3]. Discharge of wastewater with nickel content has been applied at an increasing rate in various industrial applications such as mine processing, electro-plating, melting and battery production [4, 5].

Nickel is among the most toxic materials found in environmental matrices [6]. Its permissible concentration in drinking-water is limited to  $0.01 \text{ mg/dm}^3$  in WHO and EPA guidelines due to its detrimental effects on human health [7]. Values higher than the critical level are reported to be highly toxic and carcinogenic. Such nickel levels are likely to cause lung and kidney related issues, gastrointestinal problems, and other health issues such as headache and dermatitis [8, 9].

As a non-biodegradable heavy metal, nickel exhibits high levels of toxicity in wastewater, which renders its removal from aqueous environment and the development of environment-friendly methods for its recovery, highly important [10]. Various treatment techniques including chemical precipitation, coagulation-flocculation, flotation, membrane filtering, electrochemical treatment technologies, ion exchange, evaporation and adsorption have been used for removal of heavy metals from wastewater [11-13]. Most of these techniques are not sufficiently applicable due to their drawbacks such as high operational costs, high energy consumption and production of toxic sludge.

In this context, adsorption method and psychochemical approach are proposed against this problem. Among these methods, adsorption is distinguished as one of the most efficient, cost-effective and adaptable methods for removal of heavy metals from aqueous solutions [14, 15]. Due to its ease of operation, lower costs [16] and lower amounts of resultant sludge [17], adsorption method is widely used as a traditional method for removal of heavy metals.

Particular importance has been attached to the use of alternative cost-effective materials and definition of their heavy metal removal characteristics [18]. Removal of various heavy metals using different adsorbents have been extensively studied in recent years [19-21]. For removal of nickel from wastewater, several researches have been carried out on the potential of different adsorbents such as zeolit, bentonit [22], kaolinite clay [23], coal dust and magnetized sawdust [24], teak leaves powder [25], cashew nut shell [26], *Lagenaria vulgaris* shell [27], calcareous soils [28], plantain peels [29], chitosan [30], cherry kernels [7], clay [31] and henna [16].

As one of the most popular alternative modeling techniques among evolutionary computing methods, artificial neural networks (ANN) approach, have been successfully applied to model non-linear relations involved in complex chemical processes such as adsorption [32, 33]. ANN methodology does not require an additional standard experimental design for building the model.

In this research, an ANN model, developed with experimental data, was used to estimate the effect of temperature, sorbent dosage, initial nickel concentration and initial pH on the adsorbed quantities of nickel ( $q_e$ ). Sorption isotherms, kinetics and thermodynamics were also studied. Several organic-inorganic substances were used for heavy metal removal with adsorption-biosorption, and the resulting removal efficiencies were evaluated. Differently from previous adsorption studies, chemical oxygen demand (COD) analyses were also performed depending on initial pH, sorbent dosage and temperature change, in addition to ANN modeling to determine the possible adverse effects of the sorbent.

Scanning electron microscopy (SEM), energy dispersive X-ray analysis (EDX), Fourier transform infrared (FTIR) spectroscopy, X-ray diffraction (XRD) spectrum and

atomic force microscopy (AFM) analyses were used to evaluate the interactions of peanut shell with metal ions. Each sorption experiment was performed for three times and mean values were calculated. Additionally, blank samples were used for comparison of the results throughout batch procedures. The presented results are the mean values obtained from the tests. Standard deviation ( $\text{Ni(II)} \leq 4\%$ ) values and error bars are also given.

## Material and methods

### Preparation of sorbent and solution

As the sorbent material, peanut shell was procured from domestic market in Turkey. Sorbent material was rinsed in deionized water and dried at 105 °C for a period of 24 hours. Dried peanut shell was activated after being immersed and kept in 1 %  $\text{H}_2\text{SO}_4$  solution for 24 hours. Activated sorbent was rinsed again with distilled water to remove its acidic content, and ground after being dried at 105 °C for 24 hours; afterwards it was sieved with 0.30 mm mesh size. All used chemicals were chosen among high quality analytical grade reagents.

Ni(II) solution was prepared using 4.050 g nickel chloride ( $\text{NiCl}_2 \cdot 6\text{H}_2\text{O}$ ) in 1  $\text{dm}^3$  volume so as to obtain 1000  $\text{mg}/\text{dm}^3$  concentration. Solutions with varying concentrations were prepared through making required dilutions in stock solution.

### Adsorption experiments

Adsorption of Ni(II) onto peanut shell from aqueous solution was investigated using batch equilibrium techniques. Initial pH of Ni(II) solutions was adjusted using diluted HCl or NaOH prior to the tests. The tests were performed in 250  $\text{cm}^3$  capped bials by addition of adsorbent into 100  $\text{cm}^3$  nickel solutions within specified time intervals using a temperature controlled rotating shaker. Following the shaking process, samples were subjected to centrifuge and resulting Ni(II) concentrations were measured.

Wise Shake (SHO-2D) and a shaking incubator capable of operating with the shaking speed and temperature were used throughout the research. Ni(II) ions in the samples were analyzed with Merck NOVA60 UV spectrophotometer. All pH readings were performed using Thermo Orion - STARA2145 brand pH-meter. Additionally, COD analyses were performed using standard methods.

2.0-7.0 pH interval, 5.0-100  $\text{mg}/\text{dm}^3$  initial Ni(II) concentration, 0-120 min contact time, and 0.05-1.0  $\text{g}/\text{dm}^3$  sorbent dosage are the parameters used for removal of Ni(II) ions. 0.3  $\text{g}/\text{dm}^3$  adsorbent was added to solutions with concentrations ranging between 5-100  $\text{mg}/\text{dm}^3$  at pH 7 for determination of adsorption isotherms. Also, isotherm studies were performed by adding 0.05-1  $\text{g}/\text{dm}^3$  sorbent into a solution with 25  $\text{mg}/\text{dm}^3$  concentration. Removal of Ni(II) ions was investigated at varying pH (2-7) using 3  $\text{g}/\text{dm}^3$  sorbent in 25  $\text{mg}/\text{dm}^3$  concentration.

Adsorption capacity  $q_e$  and percentage of removal efficiency  $E$  [%] were calculated using the equations:

$$q_e = \frac{V \cdot (C_o - C_e)}{x} \quad (1)$$

$$E = \frac{(C_o - C_e)}{C_o} \cdot 100 \% \quad (2)$$

where  $q_e$  is maximum adsorption capacity [mg/g];  $x$  is the adsorbent dosage [g];  $V$  is the solution's volume [cm<sup>3</sup>];  $C_o$  is the initial concentration [mg/dm<sup>3</sup>]; and  $C_e$  is the final concentration of the solution [mg/dm<sup>3</sup>].

The adsorbent kinetics of Ni(II) ions in peanut shell was analyzed using pseudo-first order, pseudo-second order, intraparticle diffusion and Elovich models. Additionally, Langmuir, Freundlich, Temkin and D-R isotherm models were used to determine the consistency of the models. The equations for isotherm models, kinetic models and thermodynamic test are given in Table 1.

Table 1

List of mathematical models

Mathematical model	Equations	Notations	
Equilibrium isotherm models			
Langmuir isotherm	$q_e = \frac{Q_o \cdot b \cdot C_e}{1 + b \cdot C_e}$ $R_L = \frac{1}{1 + b \cdot C_o}$	$q_e$ - maximum adsorption capacity $Q_o$ - denotes the maximum adsorbate uptake at equilibrium state $C_e$ - equilibrium solution concentration $b$ - Langmuir constant $C_o$ - initial concentration $R_L$ - the dimensionless equilibrium constant	[34]
Freundlich isotherm	$q_e = K_F \cdot C_e^{(1/n)}$	$K_F$ - Freundlich constant $1/n$ - adsorption intensity	[35]
Temkin isotherm	$q_e = B \ln A + B \ln C_e$	$A$ - Toth constant. The values of $A$ and $B$ can be calculated from the linear plot of $q_e$ versus $\ln C_e$	[36]
Dubinin and Radushkevich (DR) isotherm	$\ln q_e = \ln q_{max} - \beta \varepsilon^2$ $\varepsilon = RT \ln \left( 1 + \frac{1}{C_e} \right)$ $E_{ads} = \frac{1}{\sqrt{2\beta}}$	$q_e$ - maximum adsorption capacity $q_{max}$ - theoretical saturation capacity $E_{ads}$ - average adsorption energy $\beta$ - relevant activity coefficient [mol <sup>2</sup> /J <sup>2</sup> ] $\varepsilon$ - a function of Polanyi potential	[37]
Kinetics models			
Pseudo-first order model	$\log(q_e - q) = \log q_e - \frac{k_{ads,1}}{2.303} \cdot t$	$q_e$ - maximum adsorption capacity $q$ - the amount of substance adsorbed at any given $t$ time $k_{ads,1}$ - adsorption rate constant	[38]
Pseudo-second order model	$\frac{t}{q} = \frac{1}{k_{ads,2} \cdot q_e^2} + \frac{1}{q_e} \cdot t$	$k_{ads,2}$ - adsorption rate constant	[39]
Inter-particle diffusion (Weber-Morris) model	$q = k_p \cdot t^{0.5} + C$	$q$ - the amount of substance adsorbed at any given $t$ time [mg/g] $k_p$ - intra-particle diffusion constant	[40]
Elovich model	$\frac{1}{\beta} \ln(\alpha\beta) + \frac{1}{\beta} \ln t$	$\alpha$ - initial adsorption rate $\beta$ - desorption rate constant	[41]
Thermodynamic tests	$kj\Delta G^0 = \Delta H^0 - T\Delta S^0$ $\ln K_c = \frac{\Delta G^0}{R} + \frac{\Delta H^0}{RT}$	$\Delta G^0$ - Gibbs free energy [kJ/mol] $\Delta H^0$ - enthalpy exchange [kJ/mol] $\Delta S^0$ - entropy exchange [kJ/mol K] $T$ - absolute temperature [K] $\Delta G^0 = -RT \ln K_c$ ; $R$ - the gas constant with a value of 8.314 J/mol K $K_c$ - adsorption equilibrium constant $\ln K_c$ versus $1/T$ graph was plotted, $\Delta H^0$ and $\Delta S^0$ were calculated using the slope and interception point	[42]

### Artificial neural network (ANN) modeling

A neural network can be regarded as an intelligent hub with the capability to estimate an output pattern upon recognition of a given input pattern. Prior to application, neural networks are initially trained through processing of vast number of datasets. Afterwards, similarities can be detected with neural networks by use of new patterns, which in turn yields an estimated output pattern [43].

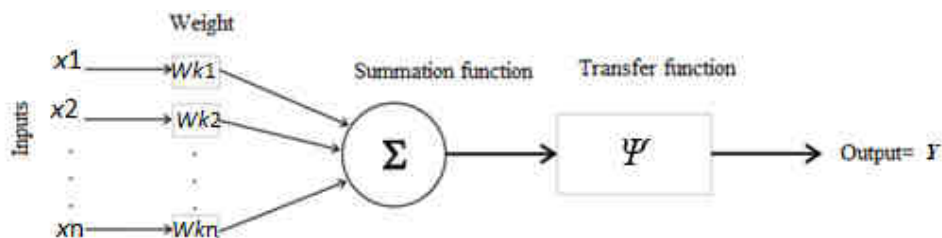


Fig. 1. ANN cell pattern

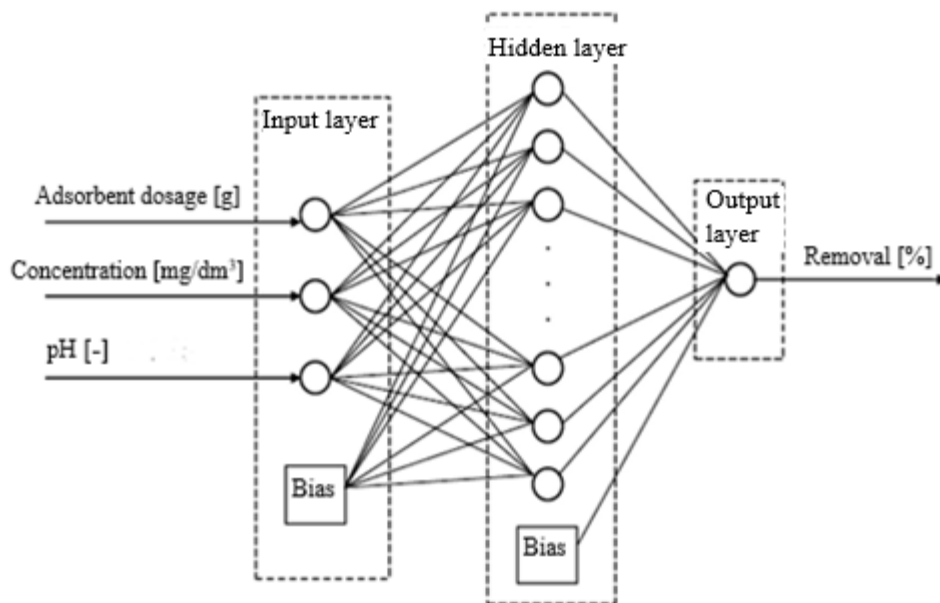


Fig. 2. Structure of a back-propagation ANN

Empirical model applications coupled with numerical estimation methods such as artificial neural network (ANN) are regarded as powerful alternatives in prediction of adsorption systems [44]. Within this scope, ANN was used for modeling adsorption using experimental data attained under varying operating conditions. A basic ANN architecture is shown in Figure 1 where inputs are symbolized with  $x_1, x_2, \dots, x_n$  and weight coefficients of inputs are symbolized with  $W_{k1}, W_{k2}, \dots, W_{kn}$ . Thus, input signals are represented with

$x_n$  and their weight coefficients are represented with  $W_{kn}$ . The weighted sum of overall input signals are given by the core.  $Y$  represents the thruputs from the network's threshold function [45].

As a training algorithm, back-propagation is widely applied in several fields, particularly in engineering applications. This method is commonly preferred due to its simple algorithm and high training capacity. Back propagation network algorithm consists of three layers, namely input, hidden and output (Fig. 2) [46, 47].

The number of hidden ANN layers can be increased depending on the essence of the problem. MATLAB software package was used during ANN calculations.

## Results and discussion

### Characterization

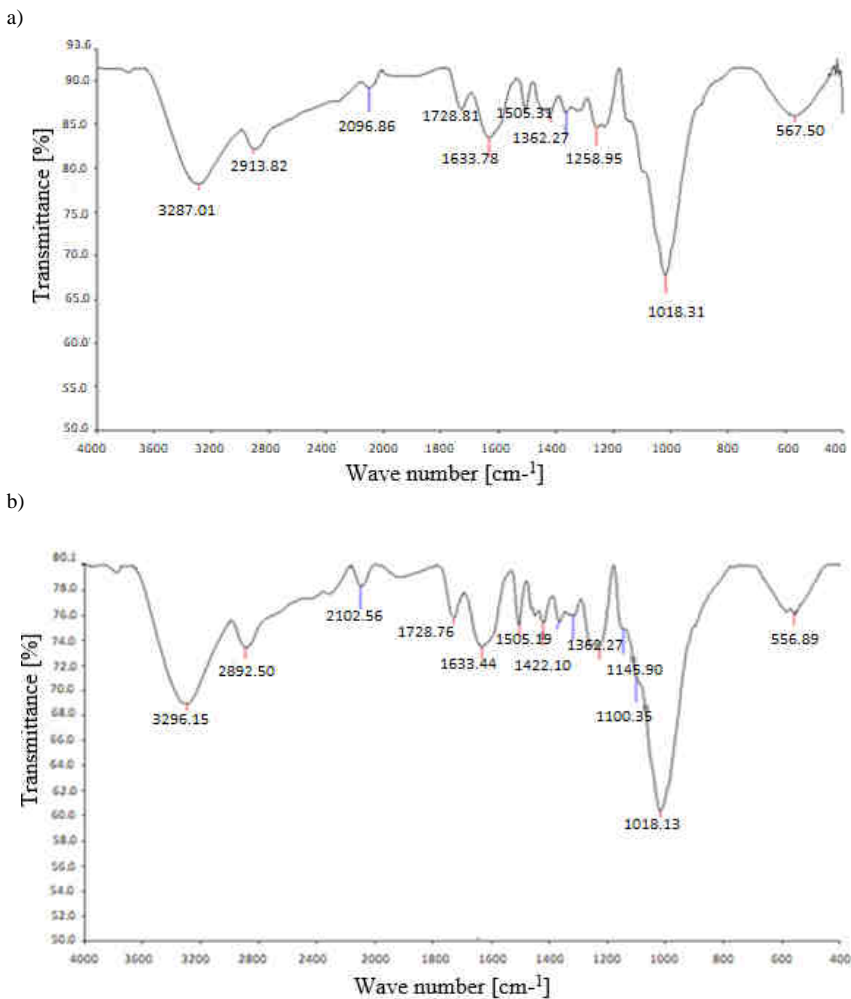


Fig 3. FTIR spectra: a) before and b) after adsorption

FTIR was used to determine the characteristics of adsorbent functional group (Fig. 3). FTIR analyses conducted following adsorption indicate some variations in adsorption peaks. According to FTIR tests, peanut shell contains various functional groups capable of adsorbing metal ions such as Ni. In general broad bands within  $3100\text{--}3550\text{ cm}^{-1}$  are associated with O-H functional group in all systems [48]. O-H functional group ( $3296\text{ cm}^{-1}$  highest) is the most effective functional group. The spectra with  $2892\text{--}2913\text{ cm}^{-1}$  wavelength relate to the functional group of  $\text{CH}_2$ .  $1728\text{ cm}^{-1}$  wavelength corresponds to the functional group of  $\text{CO}_3$ .  $1633\text{ cm}^{-1}$  wavelength peak relates to  $\text{C}=\text{O}$  functional group, whereas  $1229\text{--}1258\text{ cm}^{-1}$  wavelength corresponds to  $\text{C}=\text{N}$  functional group. The peak at  $1018\text{ cm}^{-1}$  corresponds to the functional groups of  $-\text{C}-\text{O}$  and  $-\text{S}=\text{O}$ .  $-\text{O}-\text{P}-\text{O}$  and  $-\text{PO}_4$ 's functional groups are within  $500\text{--}750\text{ cm}^{-1}$  [16].

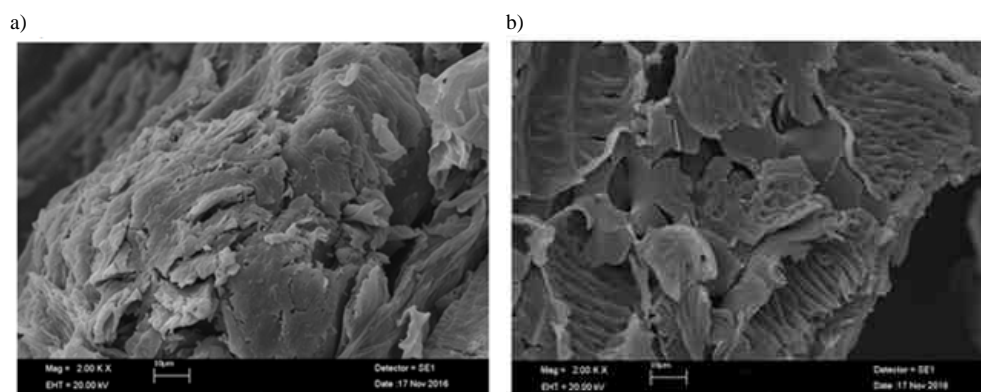


Fig. 4. SEM image of sorbent: a) before and b) after adsorption

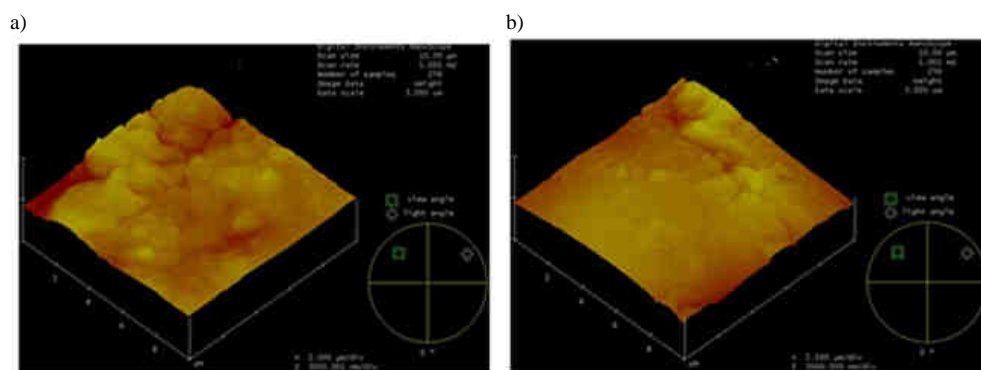


Fig. 5. AFM image of sorbent: a) before and b) after adsorption

SEM and AFM provide quantitative analyses. Surface morphologies of peanut shell before and after Ni(II) adsorption were investigated with SEM (Figs. 4a and b). As seen in Figure 4 the adsorbent surface is heterogeneous. Adsorbent pores are filled with Ni ions and bonds. This is also evident in AFM images given in Figure 5. Prior to adsorption (Fig. 5a) sorbent surface had a rough morphology whereas it became smoother after adsorption

resulting in a smoother surface (Fig. 5b). Homogenous structure of the surface is visible in AFM images. Removal right after Ni(II) adsorption can be better defined with the decrease in both local areas and overall volume of pores [49].

XRD is widely applied to define the interlayer structure of materials [50]. The sharp ridges on peanut shell, indicating its crystal and amorphous structure, are shown in the XRD spectrum given in Figure 6. Almond shell exhibited similar apices at  $16^\circ$  and  $22^\circ$ . This indicates that no structural deterioration occurred during adsorption.

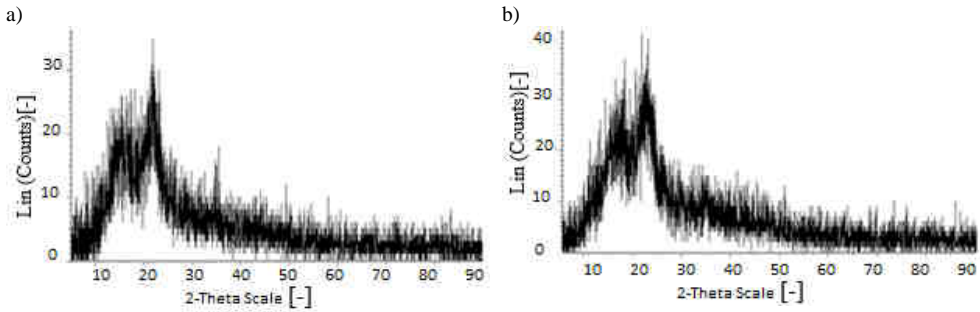


Fig. 6. XRD: a) before and b) after adsorption

### Effect of contact time

For determination of equilibrium time, following parameters were specified: initial concentration  $C_o = 25 \text{ mg/dm}^3$ , sorbent dosage ( $x$ ) 0.3 g, shaking speed = 150 rpm and pH 7. The change in Ni(II) removal with increasing contact time is shown in Figure 7.

The results indicate an increase in sorption amount with increasing contact time. However, no change was observed after 60 minutes. 60 minutes contact time was also used in some of the previous studies for removal of heavy metal with nut shell [51]; whereas longer contact times (240 min) were also reported in other studies [52].

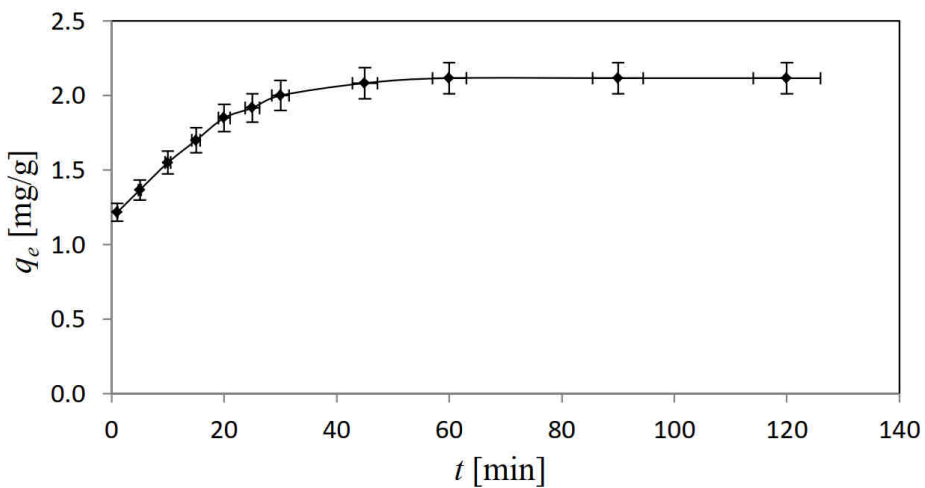


Fig. 7. Contact time

### Effect of solution pH

Figure 8a shows the removal percentage varying between pH 2 and pH 7. As seen in the figure there is no significant change between these pH values. The amount of adsorbed metal ions increased particularly after pH 4. At lower pH values, H<sup>+</sup> ions compete with metal cations for electrostatic surface charges in the system, resulting in a reduced sorption percentage [53]. In the present research, pH = 2 resulted in  $q_e = 0.42$  mg/g and 5 % efficiency values, whereas  $q_e$  was calculated as 2.12 mg/g and efficiency as 25.4 % for pH 7.

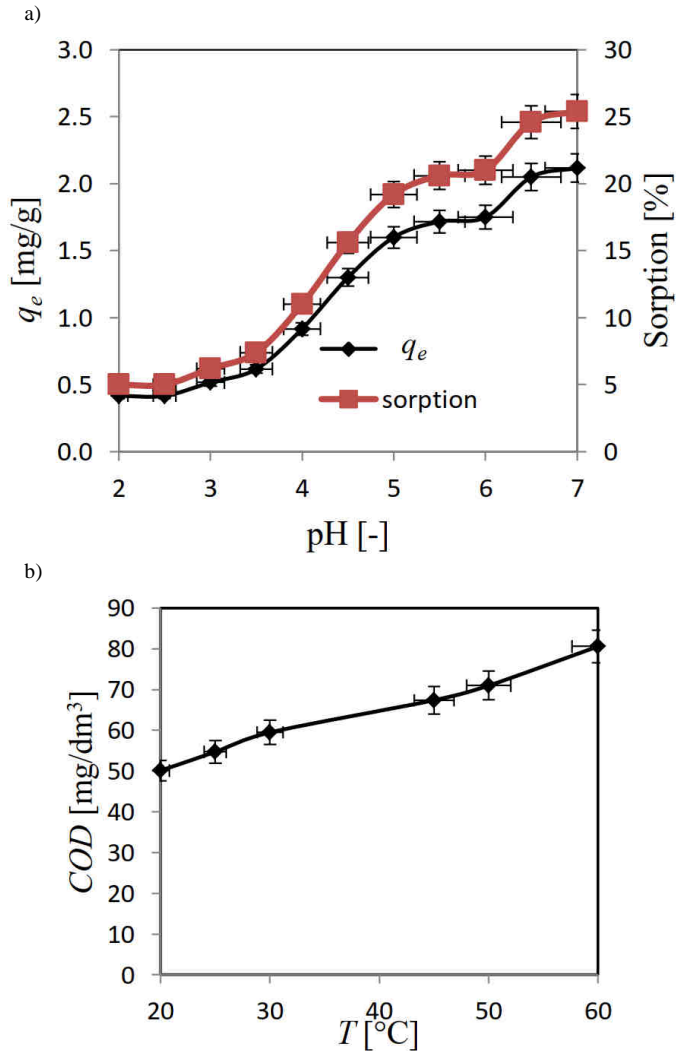


Fig. 8. Dependence: a)  $q_e$ , b) COD on pH

*COD* analyses were conducted to determine the correlation between the change in pH and the contamination induced by the sorbent (Fig. 8b). Due to the acidic media at low pH values, the sorbent degraded, resulting in higher *COD* values. *COD* was found as 96.21 mg/dm<sup>3</sup> at pH 2, and as 54.72 mg/dm<sup>3</sup> at pH 7.

### Effect of sorbent dosage

The effect of adsorbent dosage on Ni(II) removal is shown in Figure 9a. Sorbent dosages varying between 0.05 and 1 g were investigated. Increased sorbent dosage resulted in an increase in adsorption capacity and removal efficiency. 0.05 g sorbent dosage yielded 0.53  $q_e$  and 6.4 % efficiency, whereas 1 g sorbent dosage resulted in 2.38  $q_e$  and 28.6 % efficiency. Increasing adsorbent dosage relates to an increase in surface and sorption area on which metal ions are removed.

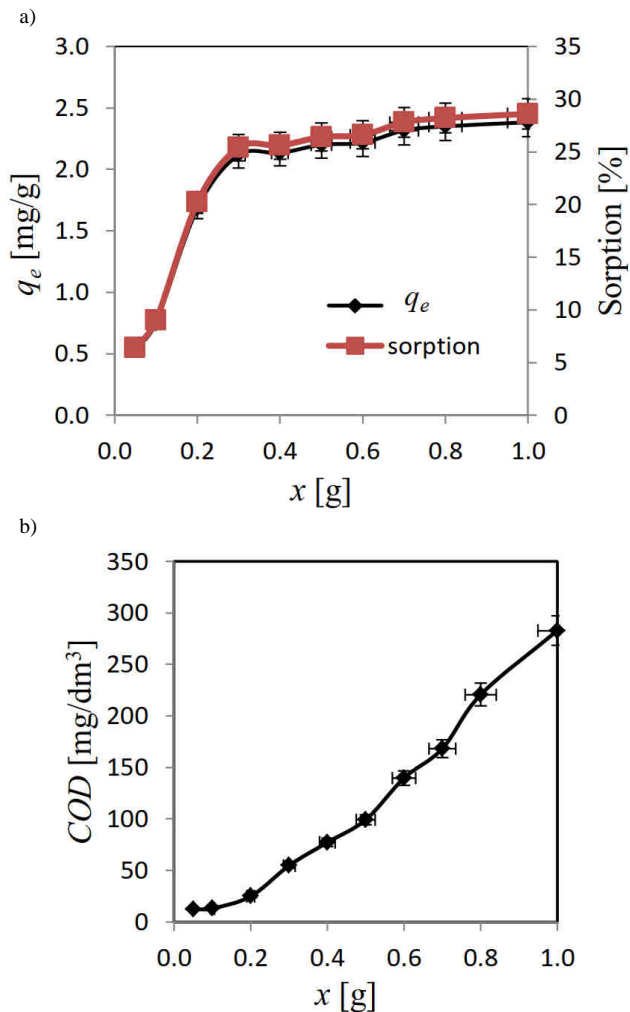


Fig. 9. Dependence: a)  $q_e$ , b) *COD* on sorbent dose

*COD* analyses were carried out to determine the possible effects of increasing sorbent dosage. As seen in Figure 9b a significant increase in *COD* value was observed with increasing sorbent dosage. *COD* value was found as 12.48 mg/dm<sup>3</sup> with 0.05 g sorbent and as 282.78 mg/dm<sup>3</sup> with 1 g sorbent.

### Effect of concentration

Experimental results of adsorption of Ni(II) ions onto peanut shell for varying concentrations (5, 15, 25, 35, 45, 60, 75, 100) are shown in Figure 10.

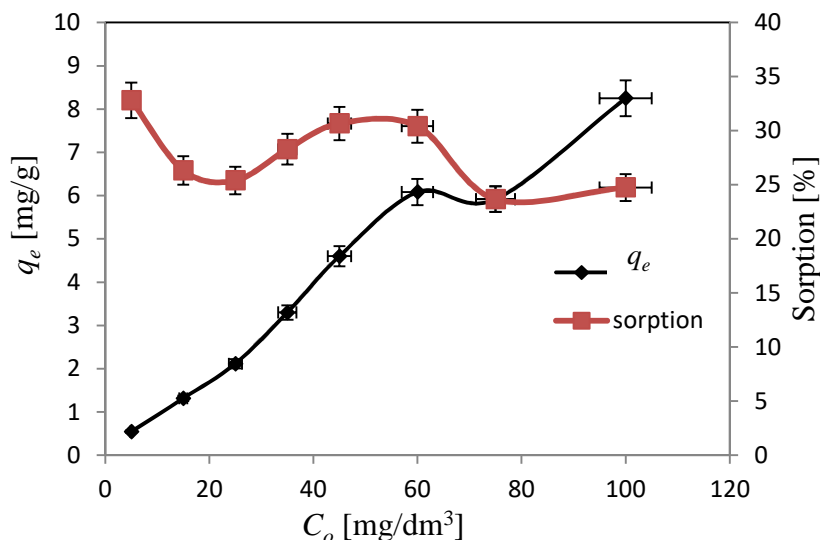


Fig. 10. Dependence  $q_e$  on concentration of Ni(II)

Removal efficiency decreased and adsorption capacity,  $q_e$  increased with the increase in nickel ion concentration. This is attributed to the increasing metal availability at the interface which in turn results in increased adsorption capacity as a result of increased metal ion concentration in the solution. As the surface-active regions are completely covered, adsorption level reaches the limit value of saturated adsorption [54]. In this study, the lowest  $q_e$  value was found as 0.55 mg/g for 5 mg/dm<sup>3</sup> ion concentration, and the highest  $q_e$  value was found as 8.25 mg/g in 100 mg/dm<sup>3</sup> concentration.

### Effect of temperature

The tests for determination of the effects of temperature on adsorption were performed between 20-60 °C (Fig. 11a). Within the interval of 20-60 °C, adsorption capacity,  $q_e$ , varied between 1.92-2.15 mg/g, and efficiency percentages varied between 23-26 %. Increased adsorption capacities with increasing temperature were reported in some of the previous studies [30, 55], whereas decreased biosorption capacities were also reported in others [56, 57]. Some researches indicated did not have any significant effect of temperature in the biosorption process [58]. Likewise, no significant effect of temperature on adsorption system was observed in the present research.

The relationship between temperature changes and *COD* was also investigated in this study. Increased *COD* values were observed as a result of increased temperatures (Fig. 11b). *COD* was specified as 50.13 mg/dm<sup>3</sup> at 20 °C, and 80.6 mg/dm<sup>3</sup> at 60 °C.

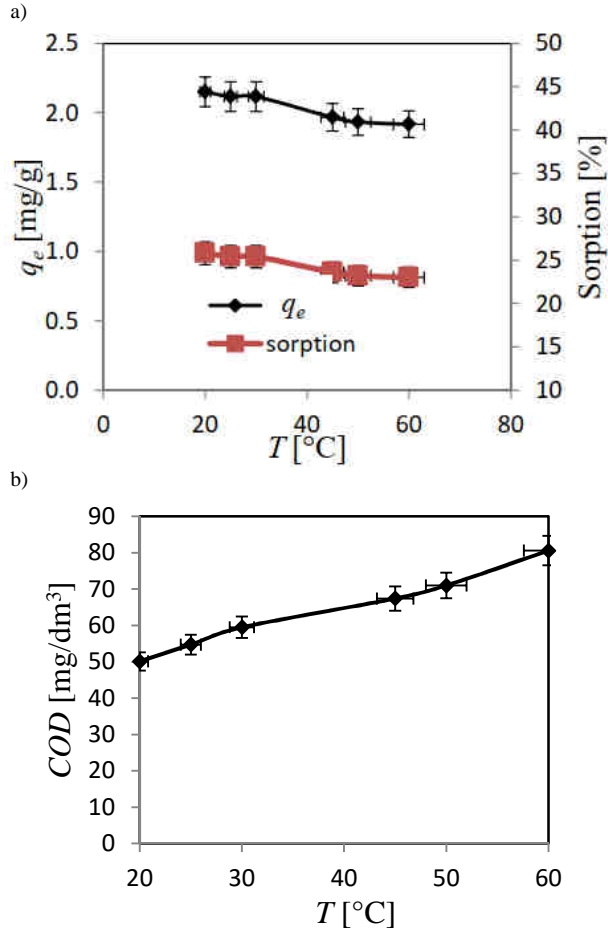


Fig. 11. Dependence: a)  $q_e$ , b) *COD* on ambient temperature

### Adsorption isotherms

The data obtained from the tests performed with different Ni(II) concentrations ( $C_o$ ) and sorbent dosages,  $x$ , were used in Langmuir, Freundlich, Temkin and D-R (Dubinin-Radushkevich) models. The coefficients obtained from these models are given in Table 2. The highest  $R^2$  value in isotherm studies was obtained with Freundlich isotherm ( $R^2 = 0.97$ ) for the initial concentration and with Temkin isotherm ( $R^2 = 0.99$ ) for sorbent dosage. This indicates an excellent agreement of data with the models. High  $R^2$  values indicate that Freundlich isotherm is suitable for definition of the multilayer Ni(II) adsorption process that occurs on a heterogeneous adsorbent surface.

Table 2

Isotherm parameters

Model	Equation	Parameters		
			$C_o$ [mg/dm <sup>3</sup> ]	$x$ [g]
Langmuir	$1/q_e = (1/Q_o \cdot b) \cdot (1/C_e) + (1/Q_o)$	$R^2$	0.30	0.93
		$b$ [dm <sup>3</sup> /mg]	0.1929	16.986
		$Q_o$ [mg/g]	0.1498	0.0099
		$R_L$	0.1717	0.0023
Freundlich	$\ln q_e = \ln K_F + (1/n) \cdot \ln C_e$	$R^2$	0.97	0.97
		$K_F$ [dm <sup>3</sup> /g]	0.4638	1170.6
		$1/n$	0.9083	5.3177
Temkin	$q_e = B \ln A + B \ln C_e$	$R^2$	0.85	0.99
		$A$ [dm <sup>3</sup> /g]	0.216	0.0393
		$B$	2.460	6.8292
D-R	$\ln q_e = \ln q_{max} - \beta e^2$	$R^2$	0.65	0.95
		$\beta$ [mol <sup>2</sup> /J <sup>2</sup> ]	-5.1523	190.44
		$q_{max}$ [mg/g]	4.1720	12.200
		$E_{ads}$ [kJ/mol]	0.3115	0.0512

Freundlich's constant ( $1/n$ ) relates to the adsorbent's density.  $0.1 < 1/n \leq 0.5$  indicates eased adsorption;  $0.5 < 1/n \leq 1$  indicates limited adsorption and  $1/n > 1$  is an indication of very low adsorption capability [59]. In this study,  $1/n$  was found as 0.9083 and 5.3177 respectively for concentration and sorbent dosage.

Also, the activation energy  $E_{ads}$  [kJ/mol] resulting from Dubinin-Radushkevich equation was found as 0.3115 and 0.0512 respectively for different concentration and sorbent dosage.  $E_{ads}$  values within 8-16 kJ/mol interval generally relate to an ion-exchange-induced sorption.  $E_{ads}$  values less than 8 kJ/mol indicate that the sorption mechanism can be defined with physical interactions [60], as in the case of the present study.

Langmuir isotherms main aim is to detect the sorption capacity. However, it should be emphasized that the isotherms can also be detected in the system of different initial concentration of the solution or different adsorbent mass [61]. In Langmuir isotherm, the type of isotherm can be inferred from separation factor  $R_L$  values ([irreversible ( $R_L = 0$ )], [favorable ( $0 < R_L < 1$ )], [linear ( $R_L = 1$ )] or [unfavorable ( $R_L > 1$ )] [62]. In this research all  $R_L$  values remain within 0-1 interval. These values signify the conformity of Langmuir isotherm to the adsorption of Ni(II) ions. However, a low  $R^2$  value was obtained during the concentration study, and a high value was obtained in the sorbent dosage study.

### Kinetics of adsorption

Kinetic tests were performed at pH 2-3-4-5-6-7 for periods ranging between 1-60 minutes (Fig. 12). The obtained data were evaluated in terms of compliance with pseudo-first order (Fig. 12a) and pseudo-second order (Fig. 12b) kinetic models, inter-particle diffusion model (Weber-Morris) (Fig. 12c) and Elovich model (Fig. 12d). Coefficients for all kinetics are given in Table 3.

Correlation coefficients for pseudo-first order kinetic model range between  $R^2 = 0.84-0.97$ . This model only applies to the area on which a very fast adsorption process takes place. According to Ho, Lagergren model is not applicable for kinetic prediction of adsorption for all adsorption periods [63].

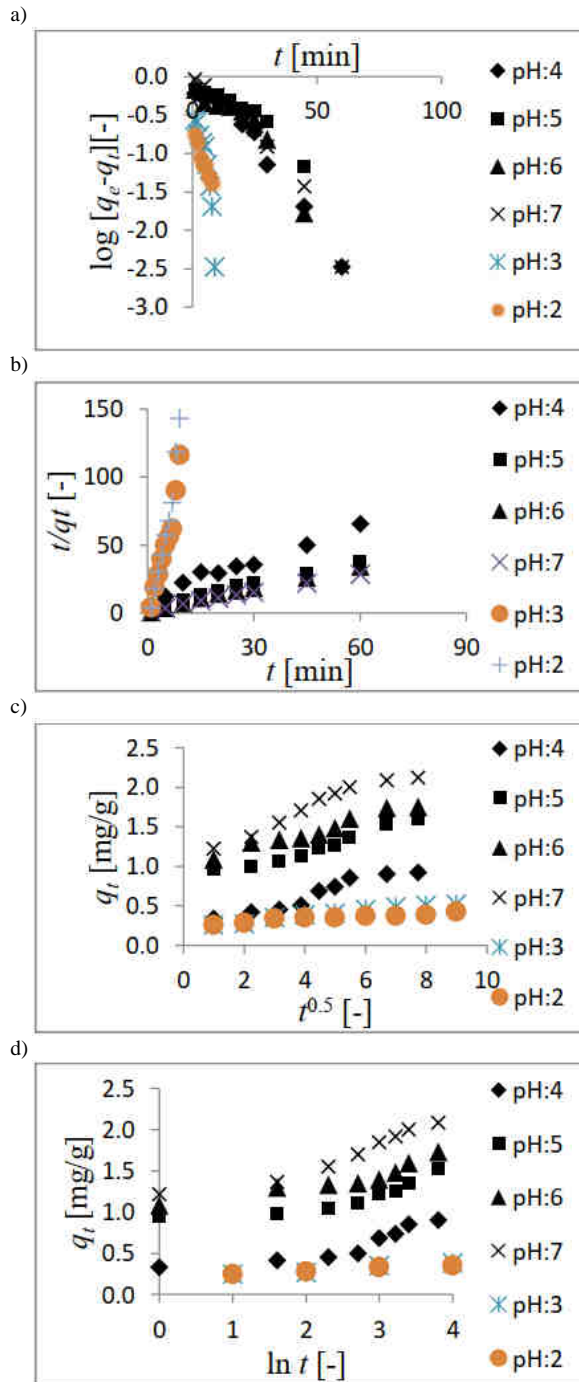


Fig. 12. Graphs of: a) pseudo-first order, b) pseudo-second order, c) Weber-Morris and d) Elovich kinetic models

Pseudo-second order equation, which is based on adsorption equilibrium capacity, is also based on the assumption that the occupancy ratio of adsorption areas are in direct proportion with the squared number of vacant areas. Adsorption ratio relates to the concentration of active areas on adsorbent surface [64]. As seen in Table 3, high regression coefficients were found for this model ( $R^2 = 0.95-0.99$ ). Also, adsorption of Ni(II) ions on peanut shell was redefined with pseudo-second order kinetic model, as the  $q_e$  values in pseudo-second order kinetic equation were very similar to the experimental results ( $q_{exp}$  [mg/g]).

Table 3

Kinetic constant for adsorption of Ni(II)

pH	$q_{exp}$ [mg/g]	Pseudo-first order			Pseudo-second order			Weber-Morris		Elovich		
		$k_1$ [min <sup>-1</sup> ]	$q_e$ [mg/g]	$R^2$ [-]	$k_2$ [g/mg·min]	$q_e$ [mg/g]	$R^2$ [-]	$k_{id}$ [mg/g·min <sup>0.5</sup> ]	$R^2$ [-]	$A$ [mg/g·min]	$B$ [g/mg]	$R^2$ [-]
2	0.42	0.033	0.141	0.87	0.844	0.420	0.99	0.023	0.93	14.46	24.87	0.94
3	0.52	0.073	0.379	0.97	0.362	0.551	0.99	0.044	0.94	1.173	13.64	0.89
4	0.92	0.090	0.920	0.95	0.101	1.050	0.95	0.101	0.92	0.603	6.238	0.81
5	1.60	0.049	0.008	0.89	0.112	1.673	0.98	0.106	0.95	22.58	6.211	0.76
6	1.75	0.074	0.981	0.84	0.157	1.816	0.99	0.099	0.95	88.97	6.207	0.87
7	2.12	0.091	0.686	0.96	0.140	2.211	0.99	0.146	0.94	21.27	4.068	0.93

Figure 12c shows the application of inter-particle diffusion model (Weber-Morris) for adsorption at varying pH conditions. The results indicate a linear correlation between  $t^{0.5}$  and overall  $q$ . Normally, if the plot coincides with the origin, this signifies that the intra-particle diffusion is only the rate limiting step. On the other hand, if the plot does not coincide with the origin, this is an indication of presence of multiple kinetic phases or sorption rates within adsorption processes [65].

Adsorption rate involves two intra-particle diffusion mechanisms. These are pore distribution or intraporous diffusion, which occurs within the volumetric boundaries of the pore; and the second is the surface diffusion which occurs on pore surfaces. Pore diffusion occurs in parallel with surface diffusion among adsorbent particles [66].

Elovich equation is successfully applied in definition of second-order kinetics based on the assumption that real solid surface is energetically heterogeneous.  $R^2$  values obtained from this model were found to be lower than those obtained from pseudo-second order model.

### Adsorption thermodynamics

In  $K_c - 1/T$  graph (Van t'Hoff graph) (Fig. 13), obtained under varying temperatures, and the thermodynamic parameters are given in Table 4. Positive  $\Delta H^0$  value signifies an endothermic reaction, and positive  $\Delta G^0$  value indicates a non-spontaneous adsorption process [67]. During the adsorption of Ni(II) ion, the increase in  $\Delta G^0$  values with increasing temperature indicates that adsorption occurs more readily at higher temperatures [68].

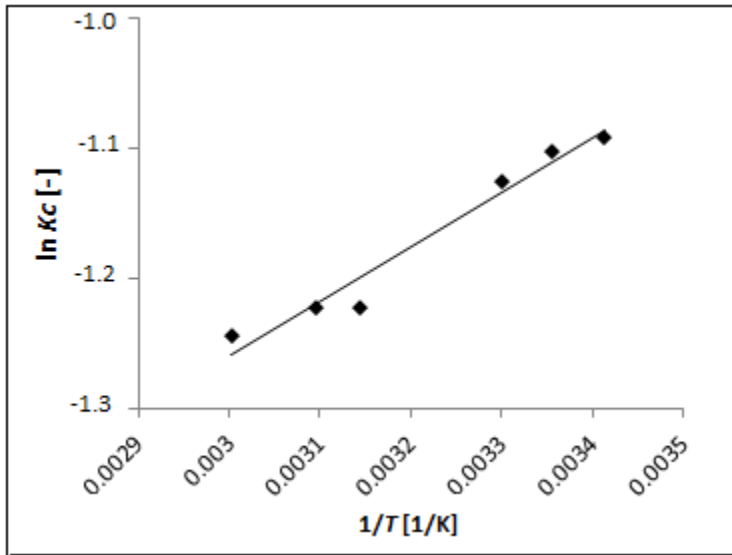


Fig. 13. Van t'Hoff graph

Table 4

Thermodynamic parameters

$\Delta H^0$ [kJ/mol]	$\Delta S^0$ [kJ/mol]	$\Delta G^0$ [kJ/K·mol]					
		293 K	298 K	303 K	318 K	323 K	333 K
3.46	-0.020	2.57	2.66	2.71	3.10	3.21	3.34

Negative  $\Delta S$  value is an indication of reduced randomness at solid/solution interface during adsorption. Low  $\Delta S$  also points to the insignificance of the changes in entropy [69].

### Adsorption mechanisms

Two fundamental mechanisms result from the interaction between adsorbent and adsorbate, namely chemical and physical adsorption. For sorption process, solute material transfer is generally characterized either by external mass transfer (boundary layer diffusion), or intra-particle diffusion, or both. The mechanism for adsorption from solution involves three steps. These are:

- 1) Diffusion of adsorbate from liquid phase towards outer surface of adsorbent.
- 2) Diffusion of adsorbate towards the pores of adsorbent.
- 3) Adsorption of adsorbate onto the pore surface of adsorbent [70] (Fig. 14).

The resistance of boundary layer is affected by the increase in adsorption rate and contact time, which results in a reduced resistance during adsorption and increased mobility of nickel [71]. Adsorption of nickel on active regions of peanut shell can be controlled via liquid phase mass transfer rate or intra-particle mass transfer rate. During the adsorption of Ni(II) onto peanut shell three consecutive stages occur which are given in Figure 14 [72].

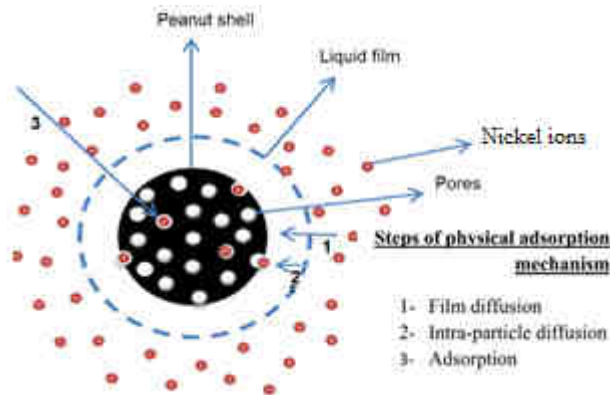


Fig. 14. Schematic diagram of the physical mechanism for adsorption of Ni(II) onto peanut shell

**Artificial neural network**

An ANN was used for modeling the adsorption studies based on the application of the experimental data at different operating conditions to train and test the neural network model. The proposed ANN type is shown in Figure 15. ANN consists of three layers: input layer, hidden layer and output layer. Solute concentration is accepted by the input layer. Hidden layer involves a group of neurons that feature a tangent sigmoid transfer function. Output layer comprises of a single neuron featuring a linear transfer function by which the adsorption capacity is calculated [73, 74]. Neurons communicate layers over weight adjusted signals. The input layer takes on signals from external sources. Weighting for each input is conducted separately in this layer and these data are sent for processing to the hidden layer. Hidden layers performed the preprocessing and the results are transferred into other hidden layers and output layers using transfer functions [75].

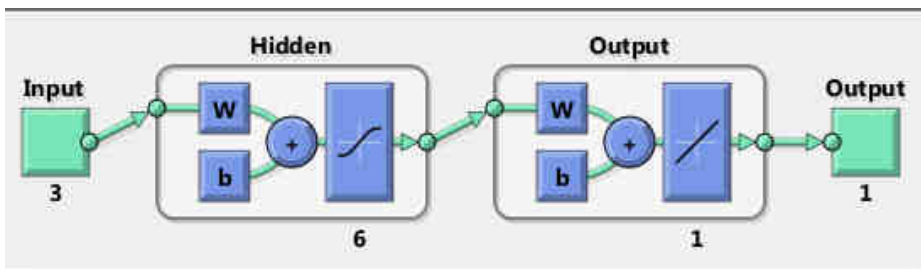


Fig. 15. ANN structure

The multilayer perceptron learns the data model using an algorithm known as “training”. These algorithms modify weights of the neurons according to the error between the values of real output and target output where provide non-linear regression between inputs and outputs variables. While number of hidden layers is to be selected depending on the complexity of the problem, but usually one hidden layer is adequate for modeling of most of the problems [76].

Experimental variables (sorbent dosage, initial concentration and initial pH) were used as input data within the built neural network to estimate the adsorbed amounts of nickel. Training, verification and test data of the ANN model that provided the best prediction are given in Figure 16. Moreover, statistical performance of the models was assessed by using the statistical parameters of mean ( $\mu$ ), standard error ( $SE$ ), standard deviation ( $\sigma$ ) and regression coefficient ( $R^2$ ). Statistical performance is provided in Table 5.

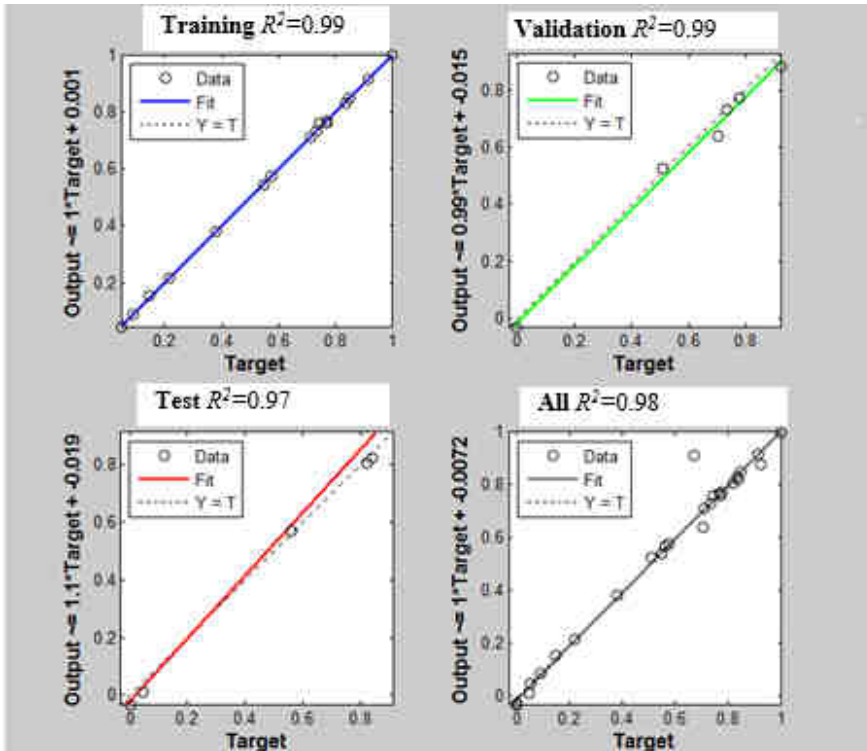


Fig. 16. Comparison of the predicted and target values in terms of Ni(II) removal percentage

Table 5

Statistical performance of the ANNs models

Model	Structure	$R^2$	$\sigma$	$SE$	$\mu$
I	3-6-1-1	0.99	8.4	2.16	1.01
II	3-5-1-1	0.97	8.4	2.24	0.99
III	3-4-1-1	0.96	8.3	1.64	1.00
IV	3-3-1-1	0.93	8.9	1.29	0.99
V	3-2-1-1	0.94	8.9	1.34	1.01

As seen in Table 5, these results indicate a significant relationship between the values observed in models created. The relationship between the prediction results of the designed ANN model and experimental data were organized so as to evaluate the success of the ANN modeling which is used as an effective tool. The comparison of the experimental results with the predicted results is given in Figure 17 (initial pH, sorbent dosage “x” and

initial concentration “ $C_o$ ”). As indicated by the figure, experimental and predicted results are in good agreement.

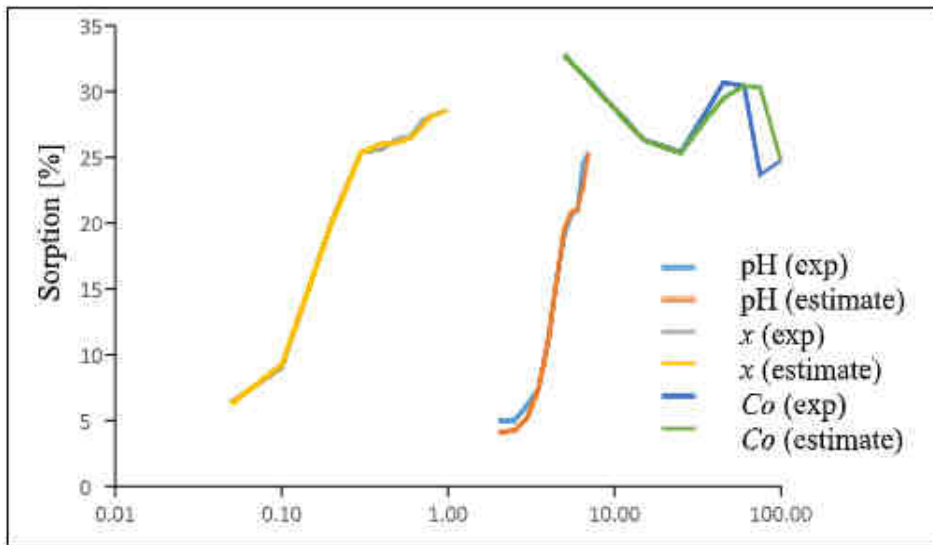


Fig. 17. Comparison of experimental results with the results predicted by the model

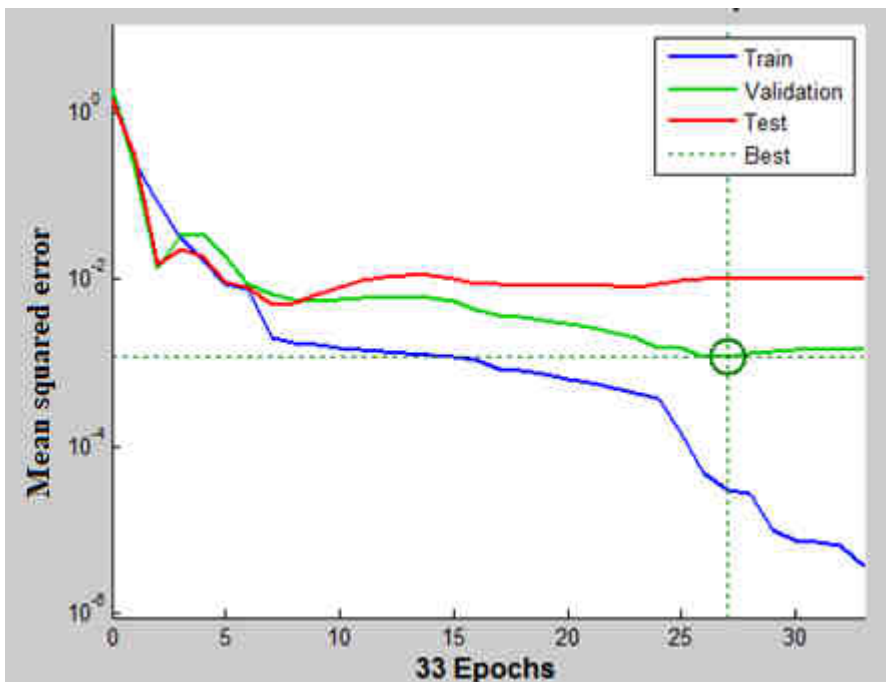


Fig. 18. MSE against the number of epochs for Ni(II)

ANN performance can be improved through normalization of the experimental data set at hand. For this particular purpose available data points were normalized to a specific level. As new data points were obtained, the developed network was retrained using these new data sets.

ANN proved to be an effective method for modeling adsorption as indicated by high  $R^2$  values ( $R^2 =$  training (0.99), test (0.97), validation (0.99)). ANN model's efficiency was determined on the basis of maximization of  $R^2$  and reduction of MSE value of the testing set (1-20 neurons correspond to the hidden layer) [77]. According to the graph for minimum mean squared error (MSE) versus the number of epochs for optimal ANN models (Fig. 18), no significant change occurs on the method's performance after 27 epochs. Best validation performance is 0.0011846 at epochs 27. As seen in Figure 18, the network is successfully trained using resilient back-propagation algorithm.

## Conclusions

In this study, the relationship between varying temperature, sorbent dosage, metal concentration and initial pH, and the adsorbed amount of nickel was predicted using an ANN model developed using experimental data. Also, the effects of metal concentrations, initial pH, temperature, contact time and sorbent dosage were determined using batch tests. To determine the possible adverse effect of the sorbent, *COD* was measured at varying temperature and pH conditions and using different sorbent dosage. The highest  $R^2$  value was obtained with Freundlich isotherm for varying concentrations ( $R^2 = 0.97$ ), and with Temkin isotherm for varying sorbent dosage ( $R^2 = 0.99$ ). High pseudo-second order kinetic model regression coefficients were obtained during kinetic studies ( $R^2 = 0.95-0.99$ ). Also, for a better definition of Ni(II) adsorption on peanut shell, adsorption was redefined with pseudo-second order kinetic model, since the  $q_e$  values in pseudo-second order kinetic equation were very similar to the experimental results ( $q_{exp}$ ). Positive  $\Delta H^0$  value in thermodynamic studies signified that the reaction was endothermic and positive  $\Delta G^0$  value was an indication of a non-spontaneous adsorption process. Negative  $\Delta S$  value, on the other hand, is attributed to a reduced randomness at the solid/solution interface during adsorption. *COD* was measured under varying temperature and pH conditions, and with varying sorbent dosage to determine the possible adverse effects of the sorbent. The sorbent degraded due to the acidic media at lower pH values, thus leading to higher *COD* values. *COD* was found as 96.21 mg/dm<sup>3</sup> at pH 2 and 54.72 mg/dm<sup>3</sup> at pH 7. Also, a significant increase in *COD* value was observed with increasing dosage of the used sorbent. *COD* was found as 12.48 mg/dm<sup>3</sup> after use of 0.05 g sorbent and as 282.78 mg/dm<sup>3</sup> after use of 1 g sorbent. Adsorption performance of peanut shell, during removal of Ni(II) from aqueous solutions was successfully predicted using a three layered neural network with 6 neurons in the hidden layer. Predicted results of the designed ANN model and the experimental data were compared and they were found to be in good agreement.

## Acknowledgement

This study and investigation has been endorsed by the Cumhuriyet University CÜBAP Chairmanship with Project No M 583. I sincerely thank CÜBAP Chairmanship for their endorsement.

## References

- [1] Çay S, Uyanik A, Özaşık A. Single and binary component adsorption of copper(II) and cadmium(II) from aqueous solutions using tea-industry waste. *Separ Purif Technol.* 2004;38(3):273-280. DOI: 10.1016/j.seppur.2003.12.003.
- [2] Tabaraki R, Nateghi A. Multimetal adsorption modeling of  $Zn^{2+}$ ,  $Cu^{2+}$  and  $Ni^{2+}$  by *Sargassum ilicifolium*. *Ecol Eng.* 2014;71:197-205. DOI: 10.1016/j.ecoleng.2014.07.031.
- [3] Zimmerman JB, Mihelcic JR, Smith J. Global stressors on water quality and quantity. *Environ Sci Technol.* 2008;42:4247-4254. DOI: 10.1021/es0871457.
- [4] Coman V, Robotin B, Ilea P. Nickel recovery/removal from industrial wastes: a review. *Resour Conserv Recycl.* 2013;73:229-238. DOI: 10.1016/j.resconrec.2013.01.019.
- [5] Malamis S, Katsou E. A review on zinc and nickel adsorption on natural and modified zeolite bentonite and vermiculite: examination of process parameters, kinetics and isotherms. *J Hazard Mater.* 2013;252-253:428-461. DOI: 10.1016/j.jhazmat.2013.03.024.
- [6] Khairy M, El-Safty SA, Shenashen MA. Environmental remediation and monitoring of cadmium. *TrAC Trend Anal Chem.* 2014;62:56-68. DOI: 10.1016/j.trac.2014.06.013.
- [7] Pap S, Radonic J, Trifunovic S, Adamovic D, Mihajlovic I, Miloradov MV, et al. Evaluation of the adsorption potential of eco-friendly activated carbon prepared from cherry kernels for the removal of  $Pb^{2+}$ ,  $Cd^{2+}$  and  $Ni^{2+}$  from aqueous wastes. *J Environ Manage.* 2016;184:297-306. DOI: 10.1016/j.jenvman.2016.09.089.
- [8] Dawodua FA, Akpomie KG. Simultaneous adsorption of Ni(II) and Mn(II) ions from aqueous solution onto a Nigerian kaolinite clay. *J Mater Res Technol.* 2014;3:129-141. DOI: 10.1016/j.jmrt.2014.03.002.
- [9] Vieira MGA, Almeida Neto AF, Gimenes ML, da Silva MGC. Removal of nickel on Bofe bentonite calcined clay in porous bed. *J Hazard Mater.* 2010;176:109-118. DOI: 10.1016/j.jhazmat.2009.10.128.
- [10] Fu F, Wang Q. Removal of heavy metal ions from wastewaters: a review. *J Environ Manage.* 2011;92:407-418. DOI: 10.1016/j.jenvman.2010.11.011.
- [11] Garba ZN, Shikin FBS, Afidah AR. Valuation of activated carbon from waste tea for the removal of a basic dye from aqueous solution. *J Chem Eng Chem Res.* 2015;2:623-633. [https://s3.amazonaws.com/academia.edu.documents/37903468/JCECR\\_PAPER.pdf?AWSAccessKeyId=AKIAIWOWYYGZ2Y53UL3A&Expires=1518191815&Signature=EuAEpe05%2BXh%2FQ4Xj1Nf2TnqKdqc%3D&response-content-disposition=inline%3B%20filename%3DValuation\\_of\\_Activated\\_Carbon\\_from\\_Waste.pdf](https://s3.amazonaws.com/academia.edu.documents/37903468/JCECR_PAPER.pdf?AWSAccessKeyId=AKIAIWOWYYGZ2Y53UL3A&Expires=1518191815&Signature=EuAEpe05%2BXh%2FQ4Xj1Nf2TnqKdqc%3D&response-content-disposition=inline%3B%20filename%3DValuation_of_Activated_Carbon_from_Waste.pdf).
- [12] Mohammadi M, Ghaemi A, Torab-Mostaedi M, Asadollahzadeh M, Hemmati A. Adsorption of cadmium(II) and nickel(II) on dolomite powder. *Desal Water Treat.* 2015;53:149-157. DOI: 10.1080/19443994.2013.836990.
- [13] Mondal S, Sinha K, Aikat K, Halder G. Adsorption thermodynamics and kinetics of ranitidine hydrochloride onto superheated steam activated carbon derived from mung seed husk. *J Environ Chem Eng.* 2015;3:187-195. DOI: 10.1016/j.jece.2014.11.021.
- [14] Qiu G, Xie Q, Liu H, Chen T, Xie J, Li H. Removal of Cu(II) from aqueous solutions using dolomite-palygorskite clay: performance and mechanisms. *Appl Clay Sci.* 2015;118:107-115. DOI: 10.1016/j.clay.2015.09.008.
- [15] Farghali AA, Bahgat M, Enaiet A, Khedr MH. Adsorption of Pb(II) ions from aqueous solutions using copper oxide nanostructures. *Beni-Suef Univ J Basic Appl Sci.* 2013;2:61-71. DOI: 10.1016/j.bjbas.2013.01.001.
- [16] Davarnejad R, Panahi P. Cu(II) and Ni(II) removal from aqueous solutions by adsorption on Henna and optimization of effective parameters by using the response surface methodology. *J Industrial Eng Chem.* 2016;33:270-275. DOI: 10.1016/j.jiec.2015.10.013.
- [17] Cao J, Wu Y, Jin Y, Yilihan P, Huang W. Response surface methodology approach for optimization of the removal of chromium(VI) by NH<sub>2</sub>-MCM-41. *J Taiwan Inst Chem Eng.* 2014;45:860-868. DOI: 10.1016/j.jtice.2013.09.011.
- [18] Akunwa NK, Muhammad MN, Akunna JC. Treatment of metal contaminated wastewater: a comparison of low-cost biosorbents. *J Environ Manage.* 2014;146:517-523. DOI: 10.1016/j.jenvman.2014.08.014.
- [19] Anna B, Kleopas M, Constantine S, Anestis F, Maria B. Adsorption of Cd(II), Cu(II), Ni(II) and Pb(II) onto natural bentonite: study in mono- and multi-metal systems. *Environ Earth Sci.* 2015;73:5435-5444. DOI: 10.1007/s12665-014-3798-0.
- [20] Sun Y, Wang Q, Chen C, Tan X, Wang X. Interaction between Eu(III) and graphene oxide nanosheets investigated by batch and extended X-ray adsorption fine structure spectroscopy and by modeling techniques. *Environ Sci Technol.* 2012;46:6020-6027. DOI: 10.1021/es300720f.

- [21] Sun YB, Zhang R, Ding CC, Wang XX, Cheng WC, Chen CL, et al. Adsorption of U(VI) on sericite in the presence of *Bacillus subtilis*: a combined batch, EXAFS and modeling techniques. *Geochim Cosmochim Acta*. 2016;180:51-65. DOI: 10.1016/j.gca.2016.02.012.
- [22] Al Dwairi R, Al-Rawajfeh A. Removal of cobalt and nickel from wastewater by using Jordan low-cost zeolite and bentonite. *J Univ Chem Technol Metall*. 2012;41:69-76. [http://dl.uctm.edu/journal/node/j2012-1/8\\_Al\\_Dwairi%20%2069-76.pdf](http://dl.uctm.edu/journal/node/j2012-1/8_Al_Dwairi%20%2069-76.pdf).
- [23] Jiang MQ, Jin XY, Lu XQ, Chen ZL. Adsorption of Pb(II), Cd(II), Ni(II) and Cu(II) onto natural kaolinite clay. *Desalination*. 2010;25:233-39. DOI: 10.1016/j.desal.2009.11.005.
- [24] Kapur M, Gupta R, Mondal MK. Parametric optimization of Cu(II) and Ni(II) adsorption onto coal dust and magnetized sawdust using Box-Behnken design of experiments. *Environ Progress Sust Energy*. 2016;35(6):1597-1604. DOI: 10.1002/ep.12393.
- [25] Vilvanathan S, Shanthakumar S. Removal of Ni(II) and Co(II) ions from aqueous solution using teak (*Tectona grandis*) leaves powder: adsorption kinetics, equilibrium and thermodynamics study. *Desalin Water Treat*. 2016;57:3995-4007. DOI: 10.1080/19443994.2014.989913.
- [26] Kumar PS, Ramalingam S, Kirupha SD, Murugesan A, Vidhyadevi T, Sivanesan S. Adsorption behavior of nickel(II) onto cashew nut shell: Equilibrium, thermodynamics, kinetics, mechanism and process design. *Chem Eng J*. 2011; 67:122-131. DOI: 10.1016/j.cej.2010.12.010.
- [27] Bojic DV, Nikolic GS, Mitrovic JZ, Radovic MD, Petrovic MM, Markovic DZ, et al. Kinetic, equilibrium and thermodynamic studies of Ni(II) ions sorption on sulfuric acid treated *lagenaria vulgaris* shell. *Chem Ind Chem Eng Q*. 2016;22(3):235-247. DOI: 10.2298/CICEQ150318037B.
- [28] Tahervand T, Jalali M. Sorption, desorption, and speciation of Cd, Ni, and Fe by four calcareous soils as affected by pH. *Environ Monit Assess*. 2016;188:322. DOI: 10.1007/s10661-016-5313-4.
- [29] Garba ZN, Nkole I, Amina U, Abdullahi K. Evaluation of optimum adsorption conditions for Ni(II) and Cd(II) removal from aqueous solution by modified plantain peels (MPP). *Beni-Suef Univ J Basic Appl Sci*. 2016;5:170-179. [https://ac.els-cdn.com/S2314853516300142/1-s2.0-S2314853516300142-main.pdf?\\_tid=19073e0a-0daa-11e8-a2f5-00000aacb361&acdnat=1518188665\\_61c173d67ac6e7dfafd0eb4aa6df7280](https://ac.els-cdn.com/S2314853516300142/1-s2.0-S2314853516300142-main.pdf?_tid=19073e0a-0daa-11e8-a2f5-00000aacb361&acdnat=1518188665_61c173d67ac6e7dfafd0eb4aa6df7280).
- [30] Liao B, Sun W, Sang-lan Ding NG, Su S. Equilibriums and kinetics studies for adsorption of Ni(II) ion on chitosan and its triethylenetetramine derivative. *Colloids and Surfaces A: Physicochem Eng Aspects*. 2016;501:32-41. DOI: 10.1016/j.colsurfa.2016.04.043.
- [31] Maleki S, Karimi-Jashni A. Effect of ball milling process on the structure of local clay and its adsorption performance for Ni(II) removal. *Appl Clay Sci*. 2017;137:213-224. DOI: 10.1016/j.clay.2016.12.008.
- [32] Khataee AR, Dehghan G, Zarei M, Ebadi A, Pourhassan M. Neural network modeling of biotreatment of triphenylmethane dye solution by a green macroalgae. *Chem Eng Res Design*. 2011;89:172-178. DOI: 10.1016/j.cherd.2010.05.009.
- [33] Das B, Mondal NK. Calcareous soil as a new adsorbent to remove lead from aqueous solution: Equilibrium, kinetic and thermodynamic study. *Uni J Environ Res Tech*. 2011;1(4):515-530.
- [34] Khan TA, Shahjahan EA. Removal of basic dyes from aqueous solution by adsorption onto binary iron-manganese oxide coated kaolinite: non-linear isotherm and kinetics modeling. *Appl Clay Sci*. 2015;107:70-77. DOI: 10.1016/j.clay.2015.01.005.
- [35] Asl SMH, Ahmadi M, Ghiasvand M, Tardast A, Katal R. Artificial neural network (ANN) approach for modeling of Cr(VI) adsorption from aqueous solution by zeolite prepared from raw fly ash (ZFA). *J Ind Eng Chem*. 2013;19:1044-1055. DOI: 10.1016/j.jiec.2012.12.001.
- [36] Allen SJ, Gan Q, Matthews R, Johnson PA. Comparison of optimised isotherm models for basic dye adsorption by kuzdu. *Bioresour Technol*. 2003;88(2):143-152. DOI: 10.1002/(SICI)1097-4660(199704)68:4<442.
- [37] Katal R, Sefti MV, Jafari M, Dehaghani AHS, Sharifian S, Ghayyem MA. Study effect of different parameters on the sulphate sorption onto nano alumina. *J Ind Eng Chem*. 2012;18:230-236. DOI: 10.1016/j.jiec.2011.11.012.
- [38] Zhang J, Cai D, Zhang G, Cai C, Zhang C, Qiu G, et al. Adsorption of methylene blue from aqueous solution onto multiporous palygorskite modified by ion beam bombardment: Effect of contact time, temperature, pH and ionic strength. *Appl Clay Sci*. 2013;83-84:137-143. DOI: 10.1016/j.clay.2013.08.033.
- [39] Ho YS, McKay G. The kinetics of sorption of basic dyes from aqueous solution by sphagnum moss peat. *Can J Chem Eng*. 1998;76(4):822-827. DOI: 10.1002/cjce.5450760419.
- [40] Murugesan A, Ravikumar L, Sathya Selva Bala V, Senthil Kumar P, Vidhyadevi T, Dnesh Kirupha S, et al. Removal of Pb(II) Cu(II) and Cd(II) ions from aqueous solution using polyazomethineamides: equilibrium and kinetic approach. *Desalination*. 2011;271:199-208. DOI: 10.1016/j.desal.2010.12.029.
- [41] Jamshidi M, Ghaedi M, Dasthian K, Hajati S, Bazrafshan AA. Sonochemical assisted hydrothermal synthesis of ZnO: Cr nanoparticles loaded activated carbon for simultaneous ultrasound-assisted adsorption

- of ternary toxic organic dye: derivative spectrophotometric, optimization, kinetic and isotherm study. *Ultrason Sonochem.* 2016;32:119-131. DOI: 10.1016/j.ultsonch.2016.03.004.
- [42] Shah J, Jan MR, Haq A, Zeeshan M. Equilibrium, kinetic and thermodynamic studies for sorption of Ni(II) from aqueous solution using formaldehyde treated waste tea leaves. *J Saudi Chemical Soc.* 2015;19(3):301-310. DOI: 10.1016/j.jscs.2012.04.004.
- [43] Enayatollahi I, Bazzazi AA, Asadi A. Comparison between neural networks and multiple regression analysis to predict rock fragmentation in open-pit mines. *Rock Mech Rock Eng.* 2014;47:799-807. DOI: 10.1007/s00603-013-0415-6.
- [44] Chairez I, Garcia-Pena I, Cabrera A. Dynamic numerical reconstruction of a fungal biofiltration system using differential neural network. *J Process Control.* 2009;19:1103-1110. DOI: 10.1016/j.jprocont.2008.12.009.
- [45] Yildiz S, Degirmenci M. Estimation of oxygen exchange during treatment sludge composting through multiple regression and artificial neural networks. *Int J Environ Res.* 2015;9(4):1173-1182. DOI: 10.22059/IJER.2015.1007.
- [46] Agarwal S, Tyagi I, Kumar GV, Ghaedi M, Masoomzade M. Kinetics and thermodynamics of methyl orange adsorption from aqueous solutions-artificial neural network-particle swarm optimization modeling. *J Molecular Liquids.* 2016;218:354-362. DOI: 10.1016/j.molliq.2016.02.048.
- [47] Ghaedi M, Zeinali N, Maghsoudi M, Purkait MK. Artificial Neural Network (ANN) method for modeling of sunset yellow dye adsorption using nickel sulfide nanoparticle loaded on activated carbon: kinetic and isotherm study. *J Dispersion Sci Tech.* 2015;36:1339-1348. DOI: 10.1080/01932691.2014.964359.
- [48] Kunnambath PM, Thirumalaisamy S. Characterization and utilization of tannin extract for the selective adsorption of Ni(II) ions from water. *Hindawi Publ Corp J Chem.* 2015;9 pages. DOI: 10.1155/2015/498359.
- [49] Zhao Y, Yang S, Ding D, Chen J, Yang Y, Lei Z, et al. Effective adsorption of Cr(VI) from aqueous solution using natural akadama clay. *J Colloid Interface Sci.* 2013;395:198-204. DOI: 10.1016/j.jcis.2012.12.054.
- [50] Zhu X, Lan L, Xiang N, Liu W, Zhao Q, Li H. Thermodynamic studies on the adsorption of  $\text{Cu}^{2+}$ ,  $\text{Ni}^{2+}$  and  $\text{Cd}^{2+}$  onto amine-modified bentonite. *Bull Chem Soc Ethiop.* 2016;30(3):357-367. DOI: 10.4314/bcse.v30i3.4.
- [51] Kiliç F, Sarici Ö, Özdemir Ç. Experimental and modeling studies of methylene blue adsorption onto particles of peanut shell. *Part Sci Tech.* 2016;34(6):658-664. DOI: 10.1080/02726351.2015.1102188.
- [52] Alothman ZA, Naushad M, Ali R. Kinetic, equilibrium isotherm and thermodynamic studies of Cr(VI) adsorption onto low-cost adsorbent developed from peanut shell activated with phosphoric acid. *Environ Sci Pollut Res.* 2013;20:3351-3365. DOI: 10.1007/s11356-012-1259-4.
- [53] Malkoc E, Nuhoglu Y. Investigations of nickel(II) removal from aqueous solutions using tea factory waste. *J Hazard Mater.* 2005;127(1-3):120-128. DOI: 10.1016/j.jhazmat.2005.06.030.
- [54] Mahramanlioglu M, Kizilcikli I, Bicer IO. Adsorption of fluoride from aqueous solution by acid treated spent bleaching earth. *J Fluorine Chem.* 2002;115(1):41-47. DOI: 10.1016/S0022-1139(02)00003-9.
- [55] Giwa AA, Abdulsalam KA, Wewers F, Oladipo MA. Biosorption of acid dye in single and multidye systems onto sawdust of locust bean (*Parkia biglobosa*) tree. *Hindawi Publish Corp J Chem.* 2016; Article ID 6436039, 11 pages. DOI: 10.1155/2016/6436039.
- [56] Maheshwari U, Mathesan B, Gupta S. Efficient adsorbent for simultaneous removal of Cu(II), Zn(II) and Cr(VI): Kinetic, thermodynamics and mass transfer mechanism. *Proc Safety Environ Protec.* 2015;98:198-210. DOI: 10.1016/j.psep.2015.07.010.
- [57] Li H, Huang G, An C, Hu J, Yang S. Removal of tannin from aqueous solution by adsorption onto treated coal fly ash: kinetic, equilibrium, and thermodynamic studies. *Ind Eng Chem Res.* 2013;52:15923-15931. DOI: 10.1021/ie402054w.
- [58] Yildiz S. Kinetic and isotherm analysis of Cu(II) adsorption onto almond shell (*Prunus dulcis*). *Ecol Chem Eng S.* 2017;24(1):87-106. DOI: 10.1515/eces-2017-0007.
- [59] Luo X, Zhang L. High effective adsorption of organic dyes on magnetic cellulose beads entrapping activated carbon. *J Hazard Mater.* 2009;171:340-347. DOI: 10.1016/j.jhazmat.2009.06.009.
- [60] Sawalha MF, Videa JRP, Gonzalez JR, Gardea-Torresdey JL. Biosorption of Cd(II), Cr(III), and Cr(VI) by saltbush (*Atriplex canescens*) biomass: Thermodynamic and isotherm studies. *J Colloid Interface Sci.* 2006;300:100-104. DOI: 10.1016/j.jcis.2006.03.029.
- [61] Klos A. Determination of sorption properties of heavy metals in various biosorbents. *Ecol Chem Eng S.* 2018;25(2): 201-216. DOI: 10.1515/eces-2018-0013.
- [62] Abd El-Latif M, Elkady M. Equilibrium isotherms for harmful ions sorption using nano zirconium vanadate ion exchanger. *Desalination.* 2010;255:21-43. DOI: 10.1016/j.desal.2010.01.020.
- [63] Ho YS, Wase DAJ, Forster CF. Kinetic studies of competitive heavy metal adsorption by sphagnum moss peat. *Environ Technol.* 1996;17:71-77. DOI: 10.1080/09593331708616362.

- [64] Li Q, Zhai J, Zhang W, Wang M, Zhou J. Kinetic studies of adsorption of Pb(II), Cr(III) and Cu(II) from aqueous solution by sawdust and modified peanut husk. *J Hazard Mater.* 2007;141:163-167. DOI: 10.1016/j.jhazmat.2006.06.109.
- [65] Vaghetti JCP, Lima EC, Royer B, Cardoso NF, Martins B, Calvete T. Pecan nutshell as biosorbent to remove toxic metals from aqueous solution. *Sep Sci Technol.* 2009;44:615-644. DOI: 10.1080/01496390802634331.
- [66] Mohan D, Singh KP. Single and multi-component adsorption of cadmium and zinc using activated carbon derived from bagasse an agricultural waste. *Water Res.* 2002;36:2304-2318. DOI: 10.1016/S0043-1354(01)00447-X.
- [67] Gupta VK, Rastogi A. Biosorption of lead from aqueous solutions by green algae *Spirogyra* species: Kinetics and equilibrium studies. *J Hazard Mater.* 2008;152:407-414. DOI: 10.1016/j.jhazmat.2007.07.028.
- [68] Kulkarni RM, Shetty KV, Srinikethan G. Cadmium(II) and nickel(II) biosorption by *Bacillus laterosporus* (MTCC 1628). *J Taiwan Inst Chem Eng.* 2014;45(4):1628-1635. DOI: 10.1016/j.jtice.2013.11.006.
- [69] Ahmad MF, Haydar S, Quraishi TA. Enhancement of biosorption of zinc ions from aqueous solution by immobilized *Candida utilis* and *Candida tropicalis* cells. *Int Biodeter Biodeg.* 2013;83:119-128. DOI: 10.1016/j.ibiod.2013.04.016.
- [70] Allen SJ, Whitten LI, Murkal M, Duggan O. The adsorption of pollutants by peat, lignite and activated chars. *J Chem Tech Biotechnol.* 1997;68(4):442-452. DOI: 10.1002/(SICI)1097-4660(199704)68:4<442.
- [71] Bulut Y, Aydin HA. Kinetics and thermodynamics study of methylene blue adsorption on wheat shells. *Desalination.* 2006;194:259-267. DOI: 10.1016/j.desal.2005.10.032.
- [72] Rehab MA, Hesham AH, Mohamed MH, Gihan FM. Potential of using green adsorbent of heavy metal removal from aqueous solutions: Adsorption kinetics, isotherm, thermodynamic, mechanism and economic analysis. *Ecol Eng.* 2016;91:317-332. DOI: 10.1016/j.ecoleng.2016.03.015.
- [73] Garza-Gonzalez MT, Alcalá-Rodríguez MM, Pérez-Elizondo R, Cerino-Córdova FJ, Garcia-Reyes RB, Loredó-Medrano JA. Artificial neural network for predicting biosorption of methylene blue by *Spirulina* sp. *Water Sci Technol.* 2011;63:977-983. DOI: 10.2166/wst.2011.279.
- [74] Gomez-Gonzalez R, Cerino-Córdova FJ, Garcia-León AM, Soto-Regalado E, Davila-Guzman. NE, Salazar-Rabago JJ. Lead biosorption onto coffee grounds: Comparative analysis of several optimization techniques using equilibrium adsorption models and ANN. *J Taiwan Inst Chem Eng.* 2011;68:201-210. DOI: 10.1016/j.jtice.2016.08.038.
- [75] Marjan T, Seyyed Hossein H, Asieh DK, Martin O, Kianoush K, Reza R, Imran A. Artificial neural network optimization form ethyl orange adsorption on topolyaniline nano-adsorbent: Kinetic, isotherm and thermodynamic studies. *J Molec Liquids.* 2017;244:189-200. DOI: 10.1016/j.molliq.2017.08.122.
- [76] Rezvan K, Fakhri Y, Mehrorang G, Kheibar D. Back propagation artificial neural network and central composite design modeling of operational parameter impact for sunset yellow and azur (II) adsorption onto MWCNT and MWCNT-Pd-NPs: Isotherm and kinetic study. *Chemomet Intelligent Lab Systems.* 2016;159:127-137. DOI: 10.1016/j.chemolab.2016.10.012.
- [77] Maghsoudi M, Ghaedi M, Zinali A, Ghaedi AM, Habibi MH. Artificial neural network (ANN) method for modeling of sunset yellow dye adsorption using zinc oxide nanorods loaded on activated carbon: Kinetic and isotherm study. *Spec Acta Part A: Molec Biomolec Spectr.* 2015;134:1-9. DOI: 10.1016/j.saa.2014.06.106.